APPLIED ORGANOMETALLIC CHEMISTRY
*Appl. Organometal. Chem.* 2001; **15**: 924–930
DOI: 10.1002/aoc.230

# Atmospheric pressure chemical vapour deposition of selenium and tellurium films by UV laser photolysis of diethyl selenium and diethyl tellurium

Josef Pola,[1]* Zdeněk Bastl,[2] Jan Šubrt[3] and Akihiko Ouchi[4]
[1]Institute of Chemical Process Fundamentals, Academy of Sciences of the Czech Republic, 165 02 Prague, Czech Republic
[2]J. Heyrovsky Institute of Physical Chemistry, Academy of Sciences of the Czech Republic, 182 23 Prague 8, Czech Republic
[3]Institute of Inorganic Chemistry, Academy of Sciences of the Czech Republic, 250 68 Řež near Prague, Czech Republic
[4]National Institute of Materials and Chemical Research, AIST, MITI, Tsukuba, Ibaraki 305, Japan

**Excimer laser-induced photolysis of gaseous diethyl selenium and diethyl tellurium $(C_2H_5)_2M$ (M = Se, Te) is controlled by cleavage of both M—C bonds, it yields $C_1$–$C_4$ hydrocarbons (ethene as major product) and results in chemical vapour deposition of selenium films and nanosized tellurium powder. The selenium and tellurium properties were characterized by X-ray photoelectron spectroscopy and Scanning electron Microscopy techniques.** 

**Keywords: diethyl selenium; diethyl tellurium; UV laser photolysis; chemical vapour deposition; selenium films; tellurium powder**

*Received 31 August 2000; accepted 15 December 2000*

## INTRODUCTION

Laser-induced chemical vapour deposition of selenium and tellurium is of lasting research interest owing to its importance for microelectronics, photographic imaging and metal–polymer optical storage media. A number of organoselenium and organotellurium compounds have potential uses as precursors. However, only a few have been examined to date.

Photodeposition of selenium films from dimethyl selenium[1,2] induced *via* radiation from mercury/xenon and mercury lamps is a very slow process due to small absorption in the precursor; this photolysis can, however, be greatly enhanced when induced by KrF laser radiation.[3]

Photodeposition of tellurium films was achieved from dimethyl and diethyl tellurium; the laser photolysis with 257 and 193 nm radiation was related to the substrate-adsorbed molecules[4,5] and the mercury/xenon lamp- and laser-induced photolyses at 193 and 248 nm with low-energy pulses were related to the gaseous molecules.[6–8] The KrF and ArF laser photolysis was disclosed to yield the ground state tellurium atoms and is presumed to involve homolysis of the Te—C bond.[6,7]

We have recently reported on ArF and KrF laser-induced photolyses of gaseous selenophene and tellurophene[9] and demonstrated[10] that these photolyses are efficient methods for chemical vapour deposition of elemental selenium and tellurium. We have also shown[11] that the prevailing pathway of the KrF laser photolysis of gaseous $(C_2H_5)_2M$ (M = Se, Te) molecules is not the M—C bond homolysis, but a four-centre molecular elimination of ethene into $MH_2$ molecules which decompose into elemental tellurium and selenium.

In this paper we report on ArF and KrF laser photolysis of diethyl selenium and KrF laser photolysis of diethyl tellurium, and centre our attention on the properties of the deposited selenium and tellurium films. We show that the

* Correspondence to: J. Pola, Laser Chemistry Group, Institute of Chemical Process Fundamentals, Academy of Sciences of the Czech Republic, 165 02 Prague 6, Czech Republic.
Email: pola@icpf.cas.cz
Contract/grant sponsor: GAAVCR; Contract/grant number: A4072107.
Contract/grant sponsor: Science and Technology Agency of Japan.

laser photolysis accomplished with high laser pulse energy is suitable for photodeposition of thin films of selenium and of sub-micrometre particles of tellurium which are not contaminated with hydrocarbon side-products.

## EXPERIMENTAL

Laser photolysis experiments were performed on gaseous samples of diethyl selenium (11 Torr) and diethyl tellurium (8 Torr) using an excimer LPX 210i laser (ArF and KrF radiation) operating at 193 and 248 nm with a repetition frequency of 10 Hz. The samples of $(C_2H_5)_2M$ (M = Se, Te) in helium (total pressure 790 Torr) were irradiated in a reactor that was equipped with a sleeve with rubber septum and PTFE valve, and consisted of two orthogonally positioned Pyrex tubes (both 3 cm in diameter), one (9 cm long) fitted with two quartz windows and the other (13 cm long) furnished with two NaCl windows. The reactor accommodated metal, quartz and KBr substrates, which were washed by acetone in an ultrasonic bath prior to use. These substrates, covered with solid materials deposited in the course of photolysis, were transferred for measurements of the deposits, properties by photoelectron spectroscopy, Fourier transform infrared (FTIR) spectroscopy and electron microscopy. The laser beam of different fluences (full width at half maximum typically 23 ns), effective over areas of 1 $cm^2$ (ArF laser) and 2.6 $cm^2$ (KrF laser), was monitored for energy output by a Gentec ED-500 joulmeter connected to a Tektronix T912 10 MHz storage oscilloscope.

The progress of the photolysis was monitored by FTIR spectroscopy (a Shimadzu FTIR 4000 spectrometer) using absorption bands at 1233 $cm^{-1}$ (diethyl selenium) and 1198 $cm^{-1}$ (diethyl tellurium), and by gas chromatography on a Gasukuro Kogyo 370 chromatograph (programmed temperature 30–150 °C, a 60 m long capillary (Neutra Bond-1) and 2 m long SUS Unipak S columns). Both chromatographs were equipped with flame-ionization detectors and connected with a Shimadzu CR 5A Chromatopac data processor. Sampling was conducted by a gas-tight syringe (Dynatech Presision Sampling). The photolytic products were identified by the gas chromatography using the comparison of retention times of products with those of authentic samples.

For the examination of the dependence of $(C_2H_5)_2Se$ and $(C_2H_5)_2Te$ depletion on the laser fluence, the entrance reactor window was cleaned before each experiment. This helped to circumvent data irreproducibility caused by a gradual decay of laser power within the reactor, which was due to some formation of selenium and tellurium films on the reactor window.

X-ray photoelectron spectroscopy (XPS) was undertaken using ESCA 3 Mk II (VG Scientific, UK) and ESCA 310 (Gammadata Scienta, Sweden) electron spectrometers, each equipped with an Al K$\alpha$ (1486.6 eV) X-ray source and operated in the fixed-analyser transmission mode. The tellurium powder was spread on a gold plate that was mounted onto a sample probe by means of tantalum clips. XP spectra were recorded both as deposited samples and after mild argon-ion etching ($E$ = 5 keV, 20 μA, 3 min) in order to remove the oxide layer grown on the surface of the sample during its transport to the spectrometer. The curve fitting of high-resolution spectra was accomplished using a Gaussian–Lorentzian line shape and a damped nonlinear least squares procedure. Quantification of the surface concentrations of elements was accomplished by correcting the photoelectron peak areas for their cross-sections.[12]

The morphology of the films was examined by scanning electron microscopy (a Tesla BS 350 ultra-high vacuum instrument) and transmission electron microscopy (a Philips 201 microscope).

Physical adsorption measurements were performed on a DigiSorb 2600 (Micromerities) volumetric instrument.

Diethyl selenium[13] and diethyl tellurium[14] were prepared using the reported procedures and distilled as a fraction with boiling points of 106 °C and 82 °C, respectively, at 100 Torr. Their purities (better than 98%) were checked by chromatography and $^1$H NMR spectroscopy. Both compounds are toxic and they were handled in a fume cupboard.

## RESULTS AND DISCUSSION

The UV absorption spectra of gaseous $(C_2H_5)_2M$ (M = Se, Te) compounds[8,11,15] reveal absorptivities at 248 nm (the wavelength of the KrF laser) for diethyl selenium of $4 \times 10^{-3}$ $Torr^{-1}$ $cm^{-1}$ and for diethyl tellurium of $7.3 \times 10^{-2}$ $Torr^{-1}$ $cm^{-1}$, and absorptivity at 193 nm (the wavelength of the ArF laser) of diethyl selenium $6.9 \times 10^{-2}$ $Torr^{-1}$ $cm^{-1}$.

The energies delivered by the 193 nm and 248 nm photons correspond to *ca* 620 kJ $Einstein^{-1}$ and 248 kJ $Einstein^{-1}$ respectively, and the dis-

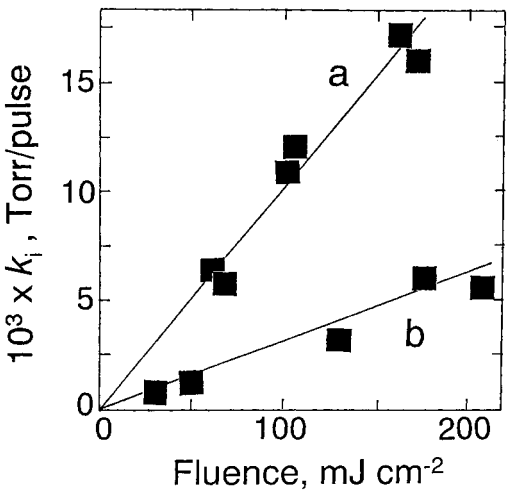


**Figure 1** Dependence of initial rate of $(C_2H_5)_2Te$ (a) and $(C_2H_5)_2Se$ (b) photolysis on KrF laser fluence. (The rate calculated corresponds to a laser beam effective area of 1 cm$^2$).

sociation energy for both the Se—C[16] and Te—C[17,18] bonds is assumed to be *ca* 250 kJ mol$^{-1}$. It is thus conceivable that absorption of the 248 nm photons is just sufficient to break both M—C bonds and that the absorption of the 193 nm photons delivers about 100 kJ mol$^{-1}$ more energy than needed to break both M—C bonds.

## Photolysis of diethyl selenium

The KrF[11] and ArF laser photolysis of diethyl selenium in excess of helium results in an instant formation of $C_1$–$C_4$ hydrocarbons and of a white fog that descends onto the reactor walls, where it creates pink films. The relative amounts of hydrocarbons are affected by the laser wavelength and incident fluence, but they do not change appreciably with photolysis progress in the range of 10–80%.

The initial depletion rate of diethyl selenium with irradiation at 248 nm (Fig. 1b) and 193 nm (Fig. 2) is linearly proportional to the laser fluence, indicating that both photolyses are a one-photon process (see also Ref 11.). Considering the difference in the effective irradiation areas (Experimental), the photolysis with the 193 nm photons is *ca* ten times faster than that with 248 nm photons; this reflects the higher absorptivity of diethyl selenium at 193 nm and also the higher energy of the 193 nm photons.

With the 248 nm radiation, the major products (in relative mole percent) are[11] ethene (80–86), *n*-butane (8–13), ethane (4–6), propane (0.5–2.0), propene (0–1.0) and methane (1–5). The values in parentheses reveal the slight variations in yields with laser fluence in the range 30–210 mJ cm$^{-2}$.

With the 193 nm radiation, the major products are ethene (43–74), *n*-butane (20–37), ethane (7–13), propane (2–6), ethyne (1–7) and methane (0–2). The values in parentheses reflect the gradual increase of ethane and *n*-butane and the decrease of ethene on increasing the laser fluence from 8 to 80 mJ cm$^{-2}$.

## Photolysis of diethyl tellurium

The KrF laser photolysis of diethyl tellurium in an excess of helium results in the formation of $C_1$–$C_2$ hydrocarbons and a dark fog that descends slowly onto the bottom of the reactor when the radiation is ceased.[11] During the irradiation, a several millimetres thick dark convection current is seen to arise in the area of the laser beam behind the reactor window; at first this moves upwards from the window and then circulates in the front area of the reactor. This feature resembles the flow of carbon particles produced in continuous-wave IR laser-induced thermolysis of hydrocarbons due to heat convection.[19]

The ArF and KrF laser photolysis of diethyl tellurium was shown to be a one-photon process at pulse energies as low as 2–6 mJ.[8] This conclusion was also drawn for KrF laser photolysis of diethyl tellurium in the absence and excess of hydro-

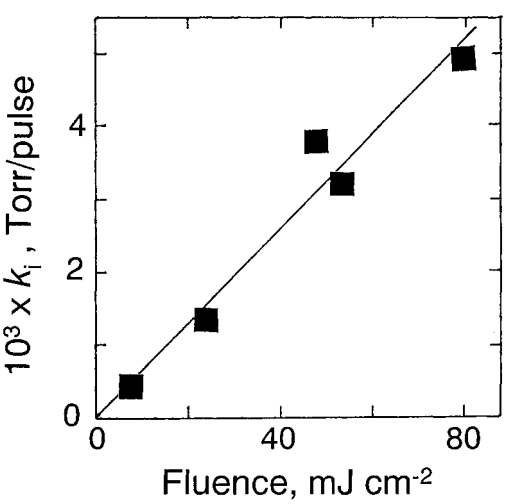


**Figure 2** Dependence of initial rate of $(C_2H_5)_2Se$ photolysis on ArF laser fluence. (The rate corresponds to a laser beam effective area of 1 cm$^2$).

gen.[6–8,20] The linear dependence of the initial depletion rate of diethyl tellurium on the laser fluence (Fig. 1a) shows (see also Ref 11.) that the KrF laser photolysis of diethyl tellurium is also a one-photon process with a pulse energy an order of magnitude higher. The efficiency of the photolysis in the range of fluence 55–160 mJ $cm^{-2}$ is demonstrated as follows: an almost complete depletion is achieved with *ca* 100 pulses at a fluence of 160 mJ $cm^{-2}$, whereas only 50% depletion can be accomplished with as many as 700 pulses at a fluence of 55 mJ $cm^{-2}$.

The relative amounts of hydrocarbons are not affected noticeably by either the laser fluence or by the photolysis progress; thus, the hydrocarbons distribution (in relative mole percent) — ethene (62–68), *n*-butane (27–20), ethane (8–10), propane (0.5–2.0), propene (0–1.0) and methane (0–2) — reflects[11] the alterations within the *ca* 10–80% photolysis progress in the range of fluence 55–160 mJ $cm^{-2}$.

## Photolysis mechanism

As shown previously,[11] the observed dominance of ethene over *n*-butane and ethane is not in keeping with the previously assumed[8–8,20] homolysis of the C—M bonds. In accordance with the known disproportionation ($2C_2H_5^{\cdot} \rightarrow C_2H_4 + C_2H_6$)/combination ($2C_2H_5^{\cdot} \rightarrow n\text{-}C_4H_{10}$) rate ratio $k_d/k_c$ for the ethyl radical ($\sim$0.13),[21] a clean M—C homolysis would have yielded *n*-butane in a large excess over equal amounts of ethane and ethene. The observed dominance of ethene over both *n*-butane and ethane reveals that more than 90% of the ethene in both the KrF and ArF laser photolyses must be produced *via* a different channel, i.e. *via* the $\beta$-elimination of ethene (Scheme 1) taking place *via* a four-centre transition state[22] (**I**).

The small amounts of propene, propane and methane and ethyne observed are in accord with unimportant radical steps (e.g. cleavage of $C_2H_5^{\cdot}$ and of reactions of $CH_3^{\cdot}$). The lower yields of ethene and higher yields of *n*-butane and ethane in the ArF laser photolysis of diethyl selenium indicate that the absorption of the higher energy 193 nm photons in the $(C_2H_5)_2Se$ molecule results, apart from the major $\beta$-elimination of ethene, in a more significant homolysis of the M—C bond.

We note that both laser photolyses of $(C_2H_5)_2M$ (M = Se, Te) proceed by a different mechanism than thermolysis of $(C_2H_5)_2$ Te, in which the $\beta$-elimination is[23] of the same importance as the expulsion of ethane from the intermediary $C_2H_5$ TeH.

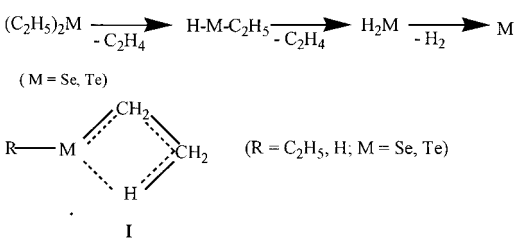


**Scheme 1**

## Properties of deposited selenium and tellurium

The deposited selenium films possess good adhesion to glass and metals (copper, aluminium), whereas the tellurium deposit forms a layer that is easily removable from the surface as powder. FTIR spectral analysis of the thin selenium films deposited on KBr do not show any absorption in the 600–4000 $cm^{-1}$ region and indicate no incorporation of $CH_n$ fragments.

XPS analysis shows that the selenium films contain selenium dioxide in the topmost layers. The observed values of the Se 3*d* core-level binding energies ($55.2 \pm 0.2$ and $59.0 \pm 0.2$ eV) are in accord[24] with those of the elemental selenium and selenium dioxide. The relative amounts of selenium and $SeO_2$ change after ion sputtering; thus *ca* 20% of selenium and 80% $SeO_2$ are present in the as-received samples, but after the removal of a layer of about 5 nm the $SeO_2$ contribution disappears and the films contain only elemental selenium (Fig. 3).

XPS measurements of the tellurium powder show that the spectrum of Te $3d_{5/2}$ photoelectrons obtained before and after argon-ion sputtering can be best fitted (Fig. 4) by two components belonging[24] to elemental tellurium and tellurium oxide and that the composition of the as-received and the sputtered sample is 14% tellurium and 86% tellurium oxide and 85% tellurium and 15% $TeO_2$ respectively.

Energy dispersive X-ray analysis reveals that, apart from oxygen, selenium and tellurium films also contain carbon in amounts estimated as below 5 at %. XPS analyses after ion sputtering result in significant decreases of carbon concentrations, indicating that carbon is contained in the topmost layers and that the materials deposited were contaminated after deposition as a result of contact

with the ambient atmosphere when transferred for analysis.

Electron microscopy analysis reveals that the morphologies of the selenium and tellurium materials differ. The deposited selenium films show a compact structure with round-shaped particles of 1–4 μm size (Fig. 5a), whereas the deposited tellurium powder shows a fluffy morphology (Fig. 5b) consisting of agglomerates of size ~100–200 nm (Fig. 5c). The observed tellurium particle size is in keeping with the measurement of physical sorption of nitrogen in tellurium powder, which showed that the tellurium particles have a BET specific surface below 20 $m^2\ g^{-1}$.

## INFERENCES

The UV laser photolysis of gaseous $(C_2H_5)_2M$ (M = Se, Te) affords chemical vapour deposition of selenium films and nanosized tellurium powder. Both processes are dominated by extrusion of M through twofold molecular elimination of ethene. The laser photolysis of $(C_2H_5)_2Se$ is more efficient with 193 nm photons than with 248 nm photons, and has a greater contribution from radical reactions.

The comparison of the laser photolytic deposition of selenium and tellurium from gaseous $(C_2H_5)_2M$ (M = Se, Te) compounds with that from selenophene[10] and tellurophene[10] is appropriate. The photolyses with both $(C_2H_5)_2M$ and $C_4H_4M$ compounds provide similar results: they afford selenium and tellurium that become oxidized in the topmost layers in air. The carbon moieties, being efficiently cleaved with each of the $(C_2H_5)_2M$ and $C_4H_4M$ compounds, yield volatile hydrocarbons that do not interfere with the deposited M. The photolysis rates (in Torr $\times 10^{-3}$ of the parent compound decomposed per pulse), at 50 mJ $cm^{-2}$ fluence and 2.6 $cm^2$ effective irradiation area — ~20 (both $C_4H_4M$, both 193 and 248 nm), 10 ($(C_2H_5)_2Se$, 193 nm), 13 ($(C_2H_5)_2Te$, 248 nm) and 3 ($(C_2H_5)_2Se$), 248 nm) — show that the cleavage of the cyclic precursors is the more efficient process.

The photolytic decomposition of the $(C_2H_5)_2M$ compounds adds to the preparation routes of selenium films by thermal[25] or laser-induced[26,27] evaporation of selenium in vacuum. The submicrometre-sized particles of tellurium produced are covered by a (>5 nm) thin layer of tellurium oxide and can find interesting uses in various

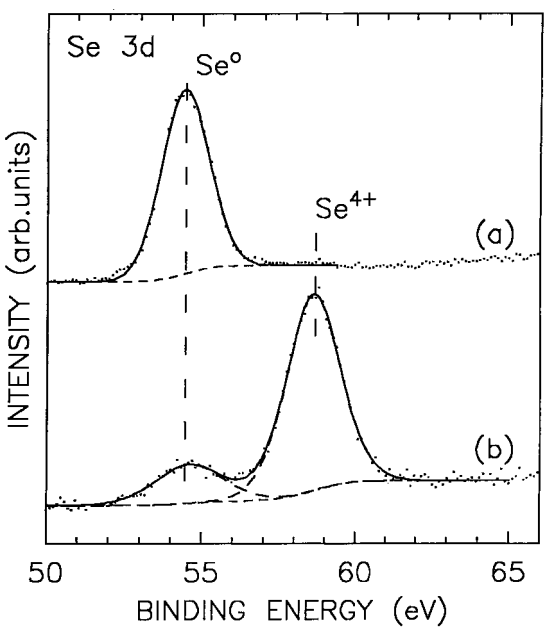


**Figure 3** Se 3*d* core-level spectra of films from $(C_2H_5)_2Se$ after (a) and before (b) ion sputtering.

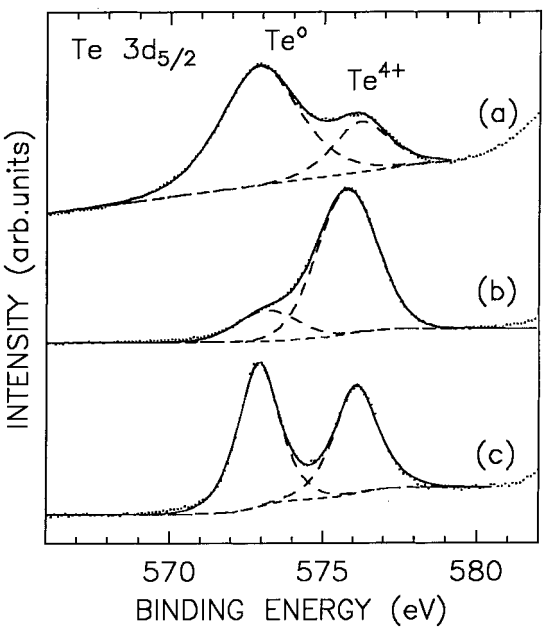


**Figure 4** Fitted photoelectron spectrum of Te $3d_{5/2}$ electrons of tellurium particles obtained from $(C_2H_5)_2Te$: (a) sputtered by argon ions; (b) as received; (c) authentic sample of tellurium exposed briefly to air.

applications. The photolytic decomposition of gaseous $(C_2H_5)_2M$ (M = Se, Te) compounds is promising for metalloorganic vapour phase epitaxy of II–VI semiconductor films[28] and for fabrication of polymeric metal-filled films for photothermal optical recording.[29] New techniques for tellurium oxide (e.g. Refs. 30, 31) and tellurium (e.g. Refs. 32–34) nano-powders are under investigation, and the reported ArF laser photolysis of diethyl tellurium can serve as a simple method of synthesis of tellurium/$TeO_2$ ultrafine powders.

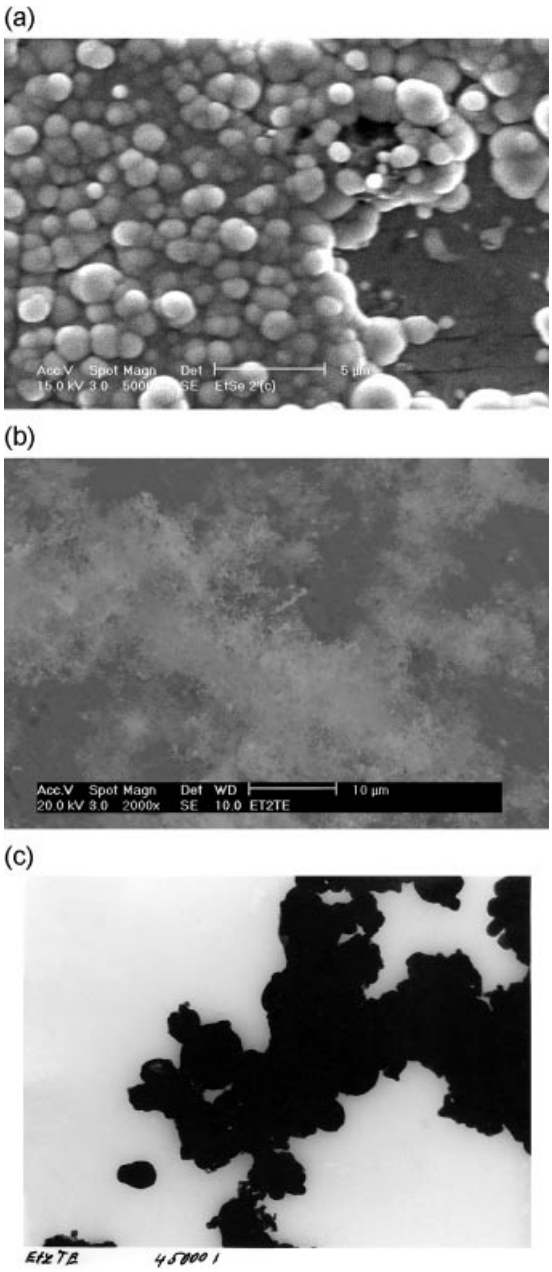


**Figure 5** Scanning electron microscopy of selenium films (a) and tellurium powder (b) transmission electron microscopy of tellurium powder (magnification ×45 000) (c).

*Acknowledgements* This work was supported by GAAVCR of the Czech Republic (grant no. A4072107) and by the Science and Technology Agency of Japan.

## REFERENCES

1. Johnson WE, Schlie LA. *Appl. Phys. Lett.* 1982; **40**: 79.
2. Ando H, Inuzuka H, Konagai M, Takahashi K. *J. Appl. Phys.* 1985; **58**: 802.
3. Pola J, Bastl Z, Subrt J, Ouchi A. *Appl. Surf. Sci.* 2001; **172**: 220.
4. Stinespring CD, Freedman A. *Appl. Phys. Lett.* 1988; **62**: 1959.
5. Irvine SJC, Hill H, Hails JE, Mullin JB, Barnett SJ, Blackmore GW, Dosser OD. *J. Vac. Sci. Technol. A* 1990; **8**: 1059.
6. Zink JJ, Brewer PD, Jensen JE, Olson GL, Tutt LW. *Appl. Phys. Lett.* 1988; **62**: 1434.
7. Jensen JE, Brewer PD, Olson GL, Tutt LW, Zink JJ. *J. Vac. Sci. Technol. A* 1988; **6**: 2805.
8. Fujita Y, Fujii S, Iuchi T. *J. Vac. Sci. Technol. A* 1989; **7**: 276.
9. Pola J, Ouchi A. *J. Org. Chem.* 2000; **65**: 2759.
10. Pola J, Bastl Z, Subrt J, Ouchi A. *Appl. Organomet. Chem.* 2000; **14**: 715.
11. Pola J, Ouchi A. *J. Organomet. Chem.* submitted for publication.
12. Scofield JH. *J. Electron Spectrosc. Relat. Phenom.* 1976; **8**: 129.
13. Bird ML, Chalenger F. *J. Chem. Soc.* 1942; 570.
14. Balfe MP, Chaplin CA, Phillips H. *J. Chem. Soc.* 1938; 341.
15. Irvine SJC, Mullin JB, Robbins DJ, Glasper JL. *J. Electrochem. Soc.* 1985; **132**: 968.
16. Batt L. *The Chemistry of Organic Selenium and Tellurium Compounds*, vol. 1, Patai S, Rappoport Z (eds). Wiley: Chichester, 1986.
17. Mullin JB, Irvine SJC. *J. Vac. Sci. Technol. A* 1986; **4**: 700.
18. McAllister T. *J. Cryst. Growth* 1989; **96**: 552.
19. Pola J. Unpublished results.
20. Brewer PD. *Chem. Phys. Lett.* 1987; **141**: 301.
21. Gibian MJ, Corley RC. *Chem. Rev.* 1973; **73**: 441.
22. Eaborn C, Mahmoud MMS, Taylor R. *J. Chem. Soc. Perkin Trans. 2* 1982; 1313.
23. Dumont H, Marbeuf A, Bouree JE, Gorochov O. *J. Mater. Chem.* 1993; **3**: 1075.
24. *NIST X-Ray Photoelectron Spectroscopy Database*, Version 2.0. US Department of Commerce, NIST Standard Reference Data Program: Gaithersburg, MD 20899, 1997.
25. Ozenbas M. *J. Mater. Sci.* 1987; **22**: 1419.

 

26. Hansen SG, Robitaille TE. *Appl. Phys. Lett.* 1987; **50**: 359.
27. Innami T, Adachi S. *Phys. Rev. B* 1999; **60**: 8284.
28. Prete P, Ahmed MU, Irvine SJC, Smith LM, Rushworth SA. *J. Mater. Sci. Mater. Electron.* 1998; **9**: 211.
29. Gritsenko KP. *Proc. SPIE–Int. Soc. Opt. Eng.* 1998; **3347**: 165.
30. El-Shall MS, Slack W, Vann W, Kane D, Hanley D. *J. Phys. Chem.* 1994; **98**: 3067.
31. Singhal A, Skandan G, Wang A, Glumac N, Kear BH, Hunt RD. *Nanostruct. Mater.* 1999; **11**: 545.
32. Tsai KL, Dye JL. *Chem. Mater.* 1993; **5**: 540.
33. Herley PJ, Jones W. *Nanostruct. Mater.* 1993; **2**: 553.
34. Yingjie Z, Yitai Q, Hai H, Manwei Z. *J. Mater. Sci. Lett.* 1996; **15**: 1700.

 